

EfficientXpert: Efficient Domain Adaptation for Large Language Models via Propagation-Aware Pruning

Songlin Zhao¹, Michael Pitts², Zhuwei Qin²

¹University of California, Berkeley

²San Francisco State University

tagorezhao@berkeley.edu, {mpitts1, zwqin}@sfsu.edu,

Abstract

The rapid advancement of large language models (LLMs) has created an increasing demand for domain-specialized variants in areas such as law, healthcare, and finance. However, their large size remains a barrier to deployment in resource-constrained environments, and existing compression methods either fail to generalize across domains or introduce high overhead. In this work, we propose **EfficientXpert**, a lightweight domain pruning framework that combines a propagation-aware pruning criterion (ForeSight Mask) with an efficient adapter update algorithm (Partial Brain Surgeon). With fine-tuning cost comparable to plain LoRA, EfficientXpert enables a one-step transformation of general pretrained models into sparse, domain-adapted experts. It achieves up to 98% of the dense model’s performance at 40% sparsity on health and legal tasks, outperforming state of the art baselines while matching LoRA’s training time and operating within 1% of LoRA’s peak GPU memory footprint.

1 Introduction

Domain-specific LLMs have advanced rapidly in recent years, driven by the growing demand in specialized domains such as law, healthcare, and finance [Song *et al.*, 2025; Zheng *et al.*, 2021; Jin *et al.*, 2019]. However, real-world deployments in these domains are often resource-constrained, as privacy and compliance requirements frequently necessitate on-premises or private-infrastructure inference. Therefore, practitioners commonly combine parameter-efficient fine-tuning (PEFT) to reduce adaptation cost with model compression techniques to reduce inference memory and computation.

PEFT enables efficient domain adaptation by updating only a small subset of parameters, often achieving performance comparable to full fine-tuning. Among PEFT approaches, Low-Rank Adaptation (LoRA) is particularly popular because it injects domain-specific behavior via low-rank updates while keeping most model weights frozen [Hu *et al.*, 2022]. However, it primarily reduces training cost: the resulting domain-adapted model largely retains the base model’s parameter count and therefore its inference-time memory

and latency overhead, which complicates deployment in resource-constrained settings. This motivates the need to compress domain-specialized LLMs in a way that preserves domain performance while reducing inference-time compute and memory requirements [Frantar and Alistarh, 2023; Han *et al.*, 2015].

One promising approach to reducing the size of LLMs is model pruning, which eliminates redundant weights to lower memory and computation costs [Han *et al.*, 2015]. Recent methods such as SparseGPT [Frantar and Alistarh, 2023] and Wanda [Sun *et al.*, 2023] demonstrate how model can retain general abilities with post-training pruning at 50% sparsity. However, applying these general-purpose pruning strategies to domain-adapted models is nontrivial. Two natural baselines are (i) pruning a domain-adapted model post hoc and (ii) pruning first and then performing PEFT; both can substantially degrade domain performance. First, as we show in Sec. 3, directly applying post training pruning to a domain adapted model can cause substantially larger performance degradation on domain tasks than on general benchmarks, suggesting that domain adaptation shifts weight saliency in ways not captured by general pruning criteria. Second, PEFT updates (e.g., LoRA) introduce dense parameter changes and do not preserve sparsity; consequently, re-enforcing the pre-PEFT pruning mask after fine-tuning is often misaligned with the adapted model and leads to significant domain-performance drops [Hu *et al.*, 2022].

To address these challenges, recent methods such as D-Pruner [Zhang *et al.*, 2024] and ATP [Lu *et al.*, 2024] incorporate domain-aware pruning and fine-tuning strategies to bridge this gap. D-Pruner uses a dual-pruning strategy that jointly considers both general and domain-specific weight importance using gradient-based approximations and regularization techniques [Zhang *et al.*, 2024]. ATP, in contrast, employs a trained pruning-decision generator, which adaptively refines model structure throughout the LoRA fine-tuning process [Lu *et al.*, 2024]. While effective, these approaches rely on gradient-based optimization and auxiliary networks, which substantially increase adaptation time and add nontrivial memory overhead, compounding the cost of an already expensive fine-tuning pipeline [Lu *et al.*, 2024; Zhang *et al.*, 2024]. Moreover, these prior methods evaluate only a limited set of tasks, whereas our broader evaluation demonstrates that pruning sensitivity depends more critically

on domain than task, highlighting a key oversight in earlier approaches.

In this work, we introduce EfficientXpert, a lightweight framework that integrates pruning with LoRA fine-tuning to produce sparse, domain-adapted LLMs. It introduces two key innovations:

- **ForeSight Mask:** A domain-aware, dynamic, gradient-free pruning method that incorporates forward error propagation into its scoring mechanism by estimating the impact of weights on downstream representations.
- **Partial Brain Surgeon:** An efficient adapter realignment step that solves a ridge regression to suppress pruned coordinates in constant time complexity, ensuring that low-rank updates stay aligned with the evolving sparse structure.

Across a comprehensive suite of health and legal tasks, EfficientXpert retains up to 99.8% and 98.43% of dense model performance at 40% sparsity on LLaMA 7B, while keeping end to end wall clock runtime within 18% of plain LoRA under the same training configuration and maintaining a comparable peak GPU memory footprint.

2 Related Work

2.1 Parameter-Efficient Fine-Tuning

As LLMs grow in size and capability, Parameter-Efficient Fine-Tuning (PEFT) has emerged as a vital strategy for adapting pretrained models to domains and downstream tasks [Li and Liang, 2021]. Among these, Low-Rank Adaptation (LoRA) has emerged as one of the most widely adopted approaches for adapting LLMs to new domains and tasks.

LoRA injects trainable low-rank matrices into the attention and feedforward layers of transformer models, enabling efficient adaptation while leaving the original weights unchanged [Hu *et al.*, 2022]. LoRA’s simplicity and strong empirical performance have driven its rapid adoption in domains such as health, law, and finance, where recent models like FinGPT [Yang *et al.*, 2023], Med-PaLM [Anil *et al.*, 2023], and LawGPT [Zhou *et al.*, 2024] successfully adapt general-purpose LLMs to specialized tasks with limited supervision and compute. Despite its success, LoRA does not reduce the size or latency of the final model, since the frozen backbone remains fully intact. Recent works have begun to explore combinations of LoRA with pruning on general tasks, seeking to preserve LoRA’s training efficiency while improving deployment efficiency [Zhang *et al.*, 2023]. However, the mechanisms by which low-rank updates capture domain- and task-specific information remain largely unexplored.

2.2 Neural Network Pruning

Pruning is a standard compression technique that removes weights while aiming to preserve task performance [Qin *et al.*, 2018; Park *et al.*, 2020]. Recent methods such as SparseGPT [Frantar and Alistarh, 2023] and Wanda [Sun *et al.*, 2023] prune pretrained LLMs using importance signals computed from general calibration data, and can retain general benchmark performance even at high sparsity.

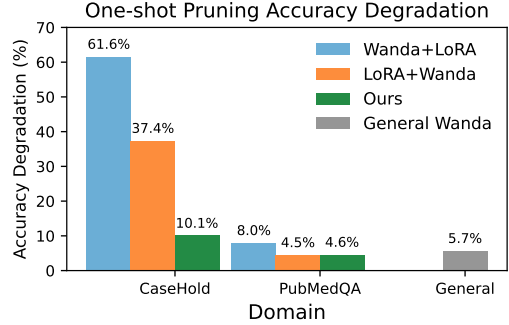


Figure 1: Accuracy degradation after single pass pruning on domain adapted LLaMA2 7B under four pipelines: Wanda then LoRA, LoRA then Wanda, our method, and Wanda with general calibration. Degradation is measured as the accuracy drop relative to the corresponding unpruned model. Results are averaged over 10 runs on two domain QA benchmarks, CaseHold and PubMedQA. The General bar is the mean accuracy degradation reported in the Wanda paper.

Domain adaptation complicates this picture. Domain data can deviate substantially from the pretraining distribution [Zhang *et al.*, 2024], and fine tuning reshapes weight and activation statistics. As a result, pruning decisions derived before fine tuning often transfer poorly to domain tasks, while pruning after domain fine tuning can also cause large domain performance drops and may require additional fine tuning to recover [Lu *et al.*, 2024; Wu *et al.*, 2025b; Wu *et al.*, 2025a; Guo *et al.*, 2025].

To address these issues, domain adaptive pruning methods such as D-Pruner and ATP update pruning decisions using domain signals during adaptation. D-Pruner combines general and domain specific importance scores via gradient based approximations and regularization to preserve domain critical weights [Zhang *et al.*, 2024]. ATP learns a pruning decision network to update masks during LoRA fine tuning and regularizes adapters to align with the evolving sparse structure [Lu *et al.*, 2024]. Although effective, both approaches add substantial overhead: gradient based scoring or auxiliary networks increase training time and introduce nontrivial GPU memory cost on top of an already expensive fine tuning pipeline.

3 Motivation

This section provides motivating evidence that general purpose post training pruning does not reliably transfer to domain adapted LLMs. We start from LLaMA2 7B hf models fine tuned with LoRA on PubMedQA (health QA) and CaseHold (legal QA), then apply Wanda at 50% sparsity using a single pass pruning step. We consider two natural pipelines: pruning before LoRA and keeping the mask fixed throughout fine tuning (Wanda+LoRA), and pruning after LoRA (LoRA+Wanda). For reference, we also include the mean accuracy degradation reported for general domain pruning in the original Wanda study.

Figure 1 reports accuracy degradation, measured as the accuracy drop relative to the corresponding unpruned model. Wanda yields substantially larger degradation on the legal domain than on the health domain, indicating that pruning be-

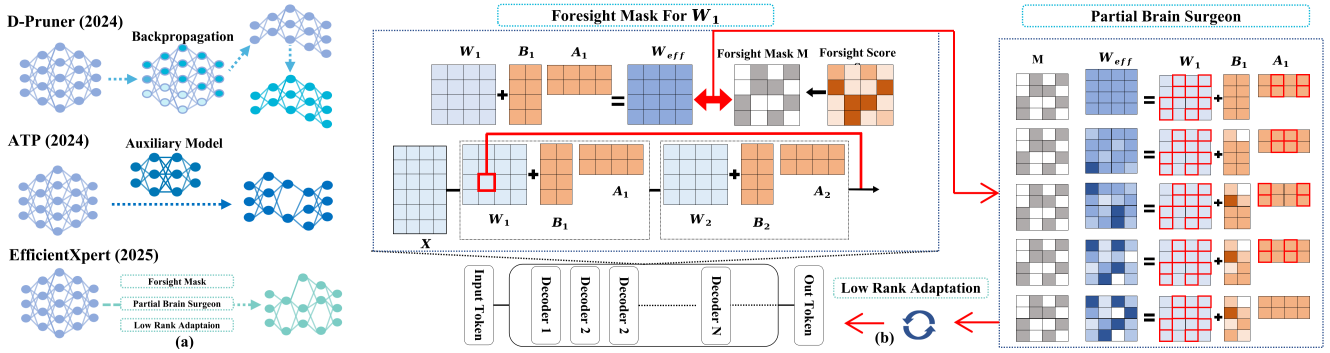


Figure 2: (a) Comparison of EfficientXpert with existing domain pruning methods. (b) Overview of EfficientXpert framework, including ForeSight Mask and Partial Brain Surgeon. EfficientXpert iteratively updates adapters, smooths importance scores, applies corrections to surviving weights, and merges the mask into dense weights to create a sparse, domain-specialized expert.

havior can vary sharply across domains after adaptation. In contrast, our method maintains low degradation across domains. These results motivate domain aware pruning strategies that account for domain induced shifts during fine tuning.

4 Methodology

To address the failure modes identified in Sec. 3, we propose EfficientXpert, which consists of two tightly coupled components. The **ForeSight Mask** dynamically determines domain-aware pruning by combining frozen general weights with evolving domain-specific adapters, selecting weights based on their impact on downstream errors without gradients. Complementing this, **Partial Brain Surgeon (PBS)** performs a post-pruning adapter recovery step: given the fixed mask, it updates the low-rank factors (e.g., updating B with A fixed) by solving a closed-form weighted ridge problem derived from a diagonal activation-norm approximation. This recovery reallocates the limited rank budget to compensate for pruning-induced loss while explicitly controlling drift on retained weights, thereby preserving domain-specific behavior that iterative gradient updates may fail to restore under tight sparsity constraints.(see Figure 2).

4.1 Notations

For clarity, we present the method on two consecutive LoRA-augmented linear layers in an MLP. The same procedure applies to all prunable weights except the final layer in each transformer block; implementation variants are provided in the Appendix B. Let $\tilde{W}_1 \in \mathbb{R}^{m \times n}$ and $\tilde{W}_2 \in \mathbb{R}^{n \times p}$ be frozen base weights with LoRA adapters (B_1, A_1) and (B_2, A_2) , where $B_1 \in \mathbb{R}^{m \times r}$, $A_1 \in \mathbb{R}^{r \times n}$, $B_2 \in \mathbb{R}^{n \times r}$, $A_2 \in \mathbb{R}^{r \times p}$, and $r \ll \min(m, n, p)$. Given input activations $X \in \mathbb{R}^{l \times m}$ with $l = \text{batch size} \times \text{sequence length}$. Here, we focus on learning a binary mask M for $\tilde{W}_1 + B_1 A_1$. Nonlinearities can be ignored without loss of generality, as justified in Appendix C.

4.2 ForeSight Mask: Propagation-Aware Pruning

Pruning upstream weights induces representation errors that propagate through subsequent layers, amplifying their downstream impact, an effect that is particularly harmful in domain-specific settings.

To explicitly account for this propagation, we score a pruning mask M for the first layer by the induced change in the two-layer output:

$$\mathcal{L}_{\text{FS}}(M) = \|X((M \odot U_1) - U_1)U_2\|_F^2, \quad (1)$$

where $U_1 := \tilde{W}_1 + B_1 A_1$, $U_2 := \tilde{W}_2 + B_2 A_2$.

From ForeSight loss to a pruning criterion. Rather than optimizing (1) directly, we derive a per-weight importance score by approximating the loss increase incurred by zeroing a single entry $\theta_{ij} := U_1[i, j]$ while holding X and U_2 fixed. Using a second-order Taylor expansion around a (local) stationary point of $\|XU_1U_2\|_F^2$ (proof in Appendix C), the predicted loss increase is

$$\Delta \mathcal{L}_{ij} \approx \frac{1}{2} \theta_{ij}^2 (X^\top X)_{ii} (U_2 U_2^\top)_{jj}. \quad (2)$$

We use (2) as the ForeSight importance score: it couples (i) the magnitude of the pruned weight, (ii) the input-energy along the affected row via $(X^\top X)_{ii}$, and (iii) the downstream amplification along the affected column via $(U_2 U_2^\top)_{jj}$.

The evolving adapters $B_1 A_1$ and $B_2 A_2$ encode early, domain-specific updates learned during finetuning. ForeSight Mask leverages these adapted effective weights through U_1 and U_2 in (1)–(2), thereby injecting domain information into pruning decisions without requiring gradient computation.

We compute this score for all weights in W_1 , and obtain the binary mask M by removing the p -th percentile of weights row-wise. For details about how group query attention mechanisms and MLP layers are handled, please refer to the Appendix.

Connection to Optimal Brain Damage. Wanda estimates weight importance from local layer statistics (e.g., weight magnitude and activation-based signals). In contrast, ForeSight derives an importance score from a second-order approximation of the downstream loss incurred by pruning an upstream weight, explicitly weighting each entry by input energy and downstream amplification. As a result, ForeSight can be viewed as an Optimal Brain Damage-style (diagonal) second-order criterion that is propagation-aware, which is particularly relevant for domain adaptation where preserving downstream fidelity is critical.

4.3 Partial Brain Surgeon

After applying the ForeSight mask M , the effective weight becomes sparse, while the LoRA adapter remains parameterized in the dense space. With fixed rank r , gradient-based training may be unable to efficiently reallocate the limited adapter capacity to the surviving subnetwork, particularly at high sparsity.

To mitigate this mismatch, we introduce a post-hoc *adapter realignment* step that updates the LoRA factor B_1 while holding A_1 fixed. Let $U_1 = W_1 + B_1 A_1$. For each output row i , we compute a rank-constrained update $\Delta b_i \in \mathbb{R}^{1 \times r}$ by solving a column-weighted ridge problem under the diagonal activation approximation $g \approx \text{diag}(X^\top X)$, with $D = \text{diag}(g)$:

$$\begin{aligned} \min_{\Delta b_i \in \mathbb{R}^{1 \times r}} \quad & \left\| (U_{1,i,S_i} + \Delta b_i A_{1,:,S_i}) D_{S_i}^{1/2} \right\|_2^2 \\ & + \left\| (\Delta b_i A_{1,:,K_i}) D_{K_i}^{1/2} \right\|_2^2 + \lambda \|\Delta b_i\|_2^2, \end{aligned} \quad (3)$$

where $S_i = \{j : M_{ij} = 0\}$ and $K_i = \{j : M_{ij} = 1\}$ denote the pruned and retained column sets in row i , and D_{S_i} and D_{K_i} are the corresponding principal submatrices of D . The parameter $\lambda > 0$ provides Tikhonov regularization.

Problem (3) admits a closed-form solution. Let $A_S := A_{1,:,S_i}$, $D_S := D_{S_i}$, $A_K := A_{1,:,K_i}$, and $D_K = D_{K_i}$. Using the decomposition $A_1 D A_1^\top = A_S D_S A_S^\top + A_K D_K A_K^\top$, we obtain

$$\Delta b_i = -U_{1,i,S_i} D_S A_S^\top \left(A_1 D A_1^\top + \lambda I_r \right)^{-1} \quad (4)$$

which can be computed efficiently by precomputing $A_1 D A_1^\top$ once per layer and solving an $r \times r$ linear system per row. Stacking the rows yields $\Delta B = [\Delta b_1^\top \cdots \Delta b_m^\top]^\top$, and we replace $B \leftarrow B + \Delta B$.

The *Partial Brain Surgeon* step suppresses pruned weights with minimal adapter perturbation, ensuring its updates remain aligned with the sparse pattern and enabling more efficient learning within the ForeSight Mask’s support.

Crucially, this correction also serves as a better initialization point for subsequent gradient updates. Under sparsity constraints, learning dynamics are highly sensitive to initialization. By steering the adapter toward domain-relevant, unpruned pathways from the outset, Partial Brain Surgeon enables more efficient adaptation and learning on the parts of the model that matter most for the target domain.

4.4 EfficientXpert Algorithm

Algorithm 1 summarises *EfficientXpert*. Starting from a pre-trained backbone, we finetune LoRA adapters on the domain corpus \mathbb{D} while simultaneously pruning with a calibration set \mathbb{D}_{cal} . At each epoch we (i) update the low-rank adapters, (ii) compute layer-wise ForeSight importance scores, (iii) smooth these scores with an Exponential Moving Average (EMA) so the mask can evolve during training, and (iv) apply a Partial Brain Surgeon (PBS) correction that retargets the adapters to the surviving weights. After the final epoch the learned mask M is merged into the dense weights, yielding a sparse, domain-specialised expert.

Algorithm 1 EfficientXpert

```

1: Input:  $f(X \mid M, W, B, A), \mathbb{D}, \mathbb{D}_{\text{cal}}, s, r, T$ 
2: Output:  $f^*$ 
3: for  $t = 1$  to  $T$  do
4:   update  $B, A$  on  $\mathbb{D}$ 
5:   for layer  $l$  do
6:      $S_t^l \leftarrow \text{ForeSight}(l, t)$ 
7:      $S^l \leftarrow \eta S_t^l + (1-\eta) S_{t-1}^l$ 
8:     remove last  $p$  fraction of entries in each row of  $S^l$ 
9:      $\Delta B^l \leftarrow \text{PBS}(S^l)$ 
10:     $B^l \leftarrow B^l + \Delta B^l$ 
11:   end for
12: end for
13: merge  $BA$  into  $W$ , apply  $M$ 
14: return  $f^*(X \mid W \odot M)$ 

```

Time Complexity ForeSight costs $\mathcal{O}(mnr)$, whereas Wanda costs $\mathcal{O}(mn)$; because $r \ll \min(m, n)$ (typically $r \in \{4, \dots, 64\}$), the additional overhead is only a small constant factor. Partial Brain Surgeon (PBS) can be executed in parallel across rows, achieving an effective *constant time* runtime in practice under sufficient compute resources. Alternatively, it can be run sequentially with $\mathcal{O}(m)$ memory, yielding a time complexity of $\mathcal{O}(mr^3)$; since r is typically small, this memory-efficient approach is practical for deployment in constrained environments. In contrast, ATP and D-Pruner invoke transformer-scale decision networks or full-gradient back-propagation, incurring $\mathcal{O}(Lmn)$ time or worse, where L is the number of transformer layers in the backbone model.

5 Experiment

Datasets Expanding on previous works, we evaluate **EfficientXpert** in two domains: **Health** and **Legal**. Each domain includes tasks such as language modeling, question answering (QA), natural language inference (NLI), and summarization. For the Health domain, we construct a training set from MedNLI, PubMedQA, and HQS at a ratio of 7:7:1, totaling 15,000 instances with a sequence length of 2048 tokens. For the Legal domain, we use CaseHold, ContractNLI, and BillSum at a 7:6:2 ratio, also totaling 15,000 instances with the same sequence length. Ratios are based on task complexity, data availability, and preliminary validation performance. Dataset details are provided in Appendix D. As shown in Section 5.4, domain calibration does not improve pruning performance on domain tasks; therefore, for a fair comparison, we use 128 C4 instances of length 2048 for both Wanda and ForeSight.

Implementation Details To assess the effectiveness and generality of our methods, We carry out a series of experiments on the LLaMA families [Touvron *et al.*, 2023] and Qwen families [Bai *et al.*, 2023], finetuning them using Low-Rank Adaptation (LoRA) with a rank of $r = 8$. LoRA adapters are attached to every weight in the models except the last linear layer. Finetuning hyperparameters are consistently set as follows: global batch size of 16, training for 3 epochs, learning rate of 1×10^{-4} , weight decay of 0.01, and the torch_Adam optimizer. Tokenization remains unchanged from the original Huggingface implementation. All finetuning and pruning were conducted on 4 NVIDIA A100

Table 1: Evaluation in the **Health** domain. Best scores are **bold**, performance surpassing dense baselines are **starred***.

Methods	Harrison	QA		NLI		HealthQuestion Summarization			Rel.% \uparrow
		Perplexity	MedNLI Acc.	MedNLI F1	PubMedQA Acc.	PubMedQA F1	R1	R2	
LLaMA2-7B (sparsity 0.5)									
Dense + LoRA	5.53	68.05	60.22	73.16	43.98	29.52	10.63	26.77	-
D-Pruner	6.74	61.88	-	-	32.58	36.49	13.71	31.85	94.57
ATP	9.53	70.51	-	-	42.06	29.66	10.36	27.38	81.38
LoRA + Wanda	6.22	64.25	41.46	64.60	47.31*	25.86	15.69	23.19	93.29
ForeSight	6.21	72.86*	54.48	69.65	49.30*	27.81	9.27	25.52	99.41
ForeSight+PBS	6.21	59.70	58.21	66.40	47.22*	27.92	9.38	24.65	94.83
LLaMA2-7B (sparsity 0.4)									
ATP	8.47	71.52	-	-	44.60	31.33	11.15	28.21	85.73
LoRA + Wanda	5.82	66.09	62.18	61.70	44.02*	26.94	9.26	24.16	94.87
ForeSight	5.82	65.21	57.66	71.95	47.84*	29.10	10.04	26.11	99.10
ForeSight+PBS	5.74	74.51*	74.83*	71.95	51.08*	30.93*	11.30*	27.74*	106.6
LLaMA3.1-8B (sparsity 0.5)									
Dense + LoRA	6.49	68.28	68.17	73.60	52.12	27.98	10.51	25.04	-
ATP	13.94	68.57	-	-	36.72	27.91	9.70	24.71	82.44
LoRA + Wanda	7.93	74.77*	56.36	71.7	50.94	26.4	9.61	23.34	96.07
ForeSight	7.92	76.09*	76.46*	71.95	51.05	27.84	10.13	23.99	103.31
ForeSight+PBS	8.16	57.42	56.34	70.55	49.53	25.80	8.85	22.95	89.40
LLaMA3.1-8B (sparsity 0.4)									
ATP	12.48	75.32	-	-	43.09	29.86	11.16	27.01	88.62
LoRA + Wanda	7.08	72.66*	54.97	73.85	52.12	26.52	9.95	23.22	96.29
ForeSight	7.08	69.03*	63.63	75.00*	52.90*	26.32	9.42	23.45	98.06
ForeSight+PBS	7.14	67.88	68.21*	73.92*	52.24*	28.20*	9.90	25.45*	99.80

GPUs with 80GB memory, using the Huggingface `peft` library for LoRA training. Models were loaded and trained in float16 precision, with gradient checkpointing enabled to reduce memory consumption. Both dense and Wanda baseline are finetuned using this setup.

Evaluation Metrics We measure language modeling performance using perplexity computed on 300 paragraphs from `InternalMed_Harrison` for the Health domain and 300 paragraphs from `en_legislation` from `MultiLegalPile` for the Legal domain. For the QA and NLI tasks, we report accuracy and F1 scores specifically on the PubMedQA, CaseHold, MedNLI, and ContractNLI datasets. For summarization tasks, the evaluation involves ROUGE-1, ROUGE-2, and ROUGE-L scores on the HQS and Billsum datasets. Model inference settings remain consistent across evaluations, with `top_k=50`, `top_p=0.9`, and `temperature=0.9`. The final reported metrics are averaged over four separate runs to ensure result robustness. We use the Huggingface datasets and evaluate libraries to compute ROUGE scores for summarization tasks. A detailed description of the evaluation datasets is provided in the Appendix. To enable a fair comparison with domain pruning methods trained on the same datasets but under different finetuning settings, we include a metric of *relative performance*, following the protocol proposed by ATP. This metric quantifies the performance of a pruned finetuned model relative to its dense counterpart under an equivalent finetuning budget. The relative performance is computed as: $\text{Rel. \%} = \left(\frac{1}{n} \sum_{i=1}^n \frac{\text{Acc}_i^{\text{pruned}}}{\text{Acc}_i^{\text{dense}}} + \frac{1}{n} \sum_{i=1}^n \frac{\text{F1}_i^{\text{pruned}}}{\text{F1}_i^{\text{dense}}} + \frac{1}{3} \sum_{j=1}^3 \frac{\text{ROUGE}_j^{\text{pruned}}}{\text{ROUGE}_j^{\text{dense}}} \right)$

n is the number of evaluation tasks, and $\text{Acc}_i^{\text{pruned}}$, $\text{Acc}_i^{\text{dense}}$, $\text{F1}_i^{\text{pruned}}$, and $\text{F1}_i^{\text{dense}}$ denote the accuracy and F1 score of the

pruned and dense models on task i . The terms $\text{ROUGE}_j^{\text{pruned}}$ and $\text{ROUGE}_j^{\text{dense}}$ correspond to the ROUGE-1, ROUGE-2, and ROUGE. All evaluations are conducted on one NVIDIA A100 GPU with 80GB of memory with model loaded at float 16 precision.

5.1 Baselines

Dense + LoRA We finetune the LLaMA and Qwen model families using the LoRA configuration described above; results for the Qwen models are provided in the Appendix.

LoRA + Wanda Based on the findings in Section 3, we apply Wanda [Sun *et al.*, 2023] after LoRA finetuning, which yields the strongest performance among the considered baselines. All domain-specific training datasets, LoRA finetuning settings, and evaluation metrics follow Section 5.

D-Pruner and ATP. We also compare **EfficientXpert** with two state-of-the-art domain pruning methods: D-Pruner [Zhang *et al.*, 2024] and ATP [Lu *et al.*, 2024]. Since our evaluation spans a broader range of tasks and datasets than prior work, we report previously published results as-is and compare only relative performance scores, which provide a fair basis for cross-setting comparisons.

5.2 Main Results

Health Domain

In the health domain, EfficientXpert consistently outperforms prior pruning baselines, including Wanda, ATP, and D-Pruner. Across model sizes and sparsity levels, EfficientXpert consistently outperforms existing methods in preserving Harrison perplexity and HQS summarization performance. At a sparsity level of 0.4, EfficientXpert augmented with the ForeSight mask and Partial Brain Surgeon (PBS) attains relative performance of 106.6% on LLaMA2-7B and 99.80% on

Table 2: Evaluation in the **Legal** domain. Best pruned scores are **bold**, performance surpassing dense baselines are **starred***.

Methods	MultiLegalPile Perplexity	QA		NLI		Billsum Summarization			Rel.% \uparrow
		ContractNLI Acc.	ContractNLI F1	CaseHold Acc.	CaseHold F1	R1	R2	RL	
LLaMA2-7B (sparsity 0.5)									
Dense + LoRA	3.84	75.84	72.50	70.62	68.19	32.71	13.93	18.30	-
D-Pruner	2.73	-	-	-	27.58	31.00	19.03	25.96	93.53
ATP	3.67	-	-	-	-	43.18	23.12	30.06	81.99
LoRA + Wanda	4.35	53.60	46.73	41.33	41.15	33.31*	11.50	17.79	69.57
ForeSight	4.10	71.37	68.38	63.5	63.46	34.11*	11.94	18.43*	93.65
ForeSight+PBS	4.02	69.61	67.12	63.5	63.49	33.94*	12.04	18.43*	92.86
LLaMA2-7B (sparsity 0.4)									
ATP	2.82	-	-	-	-	43.8	23.12	30.06	91.23
LoRA + Wanda	4.09	57.62	49.90	46.12	46.35	35.33*	11.83	18.67*	75.28
ForeSight	3.96	77.4*	74.99*	68.5	68.50	37.65*	13.81	19.94*	100.52
ForeSight+PBS	3.88	74.13	70.35	70.5	70.36*	37.47*	13.61	19.91*	100.96
LLaMA3.1-8B (sparsity 0.5)									
Dense + LoRA	4.44	76.14	74.97	82.5	68.65	33.64	15.58	19.66	-
ATP	4.28	-	-	-	-	43.1	22.6	28.65	82.44
LoRA + Wanda	5.35	50.18	39.60	41.5	41.58	35.05*	12.83	19.11	64.83
ForeSight	5.32	72.37	71.27	67.5	67.06	37.81*	14.62	20.56*	94.73
ForeSight+PBS	5.38	74.38	71.94	68	67.71*	35.03*	13.24	19.52	94.61
LLaMA3.1-8B (sparsity 0.4)									
ATP	4.13	-	-	-	-	45.28	25.45	30.15	88.62
LoRA + Wanda	4.83	59.46	48.30	62.5	62.28	35.54*	14.05	20.16*	81.69
ForeSight	4.85	75.60	74.29	73.15	72.94*	35.38*	14.08	19.86*	98.43
ForeSight+PBS	4.82	77.05*	74.97*	64	63.48	35.77*	14.18	20.23*	94.26

Table 3: Qwen 8B Health EfficientXpert Runtime and Memory.

Prune%	Total Runtime	Peak Memory	Health ppl
-	74 mins	67949.30 MiB	8.4086
40%	94 mins	71239.47 MiB	8.0113
50%	94 mins	67949.30 MiB	8.7747

LLaMA3.1-8B, exceeding the dense baseline. At a higher sparsity level of 0.5, EfficientXpert with ForeSight alone remains robust, achieving 99.41% (LLaMA2-7B) and 103.31% (LLaMA3.1-8B) relative performance. Moreover, EfficientXpert maintains a larger margin over Wanda as sparsity increases, as shown in Figure 3(a).

Legal Domain

Notably, EfficientXpert (with or without PBS) consistently outperforms domain pruning baselines such as ATP and D-Pruner in relative performance across all evaluated sparsity levels and model scales. Moreover, EfficientXpert exceeds the general pruning method Wanda by a substantial margin on every task at every sparsity level (Figure 3(b)), demonstrating stronger adaptation to domain-specific objectives. At $p = 0.4$ on LLaMA2-7B, EfficientXpert even surpasses the dense baseline: ForeSight achieves 100.54% relative performance, while ForeSight+PBS reaches 100.96%. Finally, we observe that EfficientXpert is particularly effective at preserving summarization quality and low perplexity.

5.3 Efficiency Analysis

Tables 4 and 3 report end-to-end wall-clock runtime, average peak GPU memory, and in-domain perplexity for Qwen 8B adapted through EfficientXpert pipeline (ForeSight Mask +

Table 4: Qwen 8B Legal EfficientXpert Runtime and Memory.

Prune%	Total Runtime	Peak Memory	Legal ppl
-	106 mins	45728.68 MiB	5.1969
40%	125 mins	46277.05 MiB	5.4110
50%	125 mins	45990.94 MiB	5.8528

PBS). Across both the legal and health domains, EfficientXpert incurs only modest additional finetuning time relative to dense LoRA (e.g., 125 vs. 106 minutes on Legal, $\sim 18\%$ overhead) while maintaining essentially the same peak memory footprint (within $\sim 1\%$ when averaged over four GPUs). These observations align with the complexity analysis in Sec. 4.4 and suggest that EfficientXpert delivers inference-efficient sparse domain models without the substantial training-time or memory costs typical of prior domain-pruning approaches such as ATP and D-Pruner.

5.4 Ablation

Higher LoRA rank improves Partial Brain Surgeon

When the recovery rank (r) is small relative to the number of pruned entries $|S_i|$, the reconstruction has limited degrees of freedom and may not fully compensate for pruning-induced errors. Increasing (r) expands the expressive capacity of PBS, enabling more accurate recovery, especially at higher sparsity levels, where the number of pruned entries grows. We evaluate this effect by varying (r) at 50% sparsity on Llama-3.2-1B. Figure 3 shows a clear and consistent trend: larger ranks yield higher relative performance.

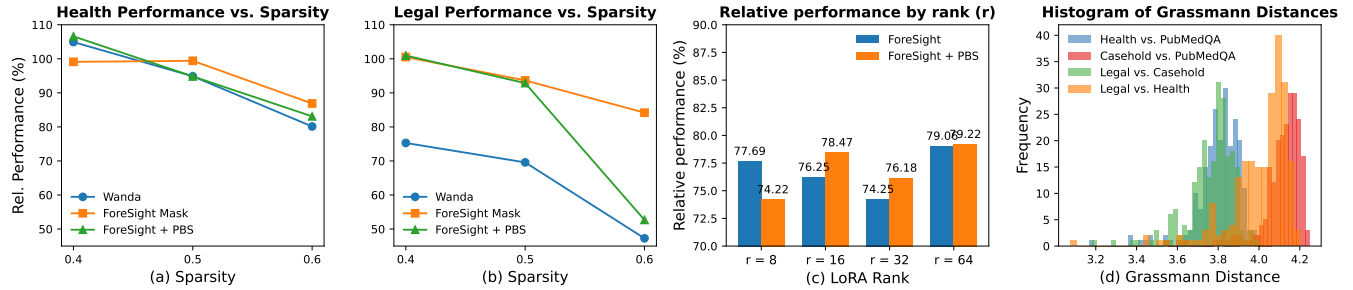


Figure 3: (a–b) LLaMA2-7B relative performance vs. sparsity on Health and Legal for Wanda, FORESIGHT, and FORESIGHT+PBS. (c) Post-pruning Rel. Performance as a function of LoRA rank r . (d) Grassmann-distance histograms contrasting task shifts with domain shifts.

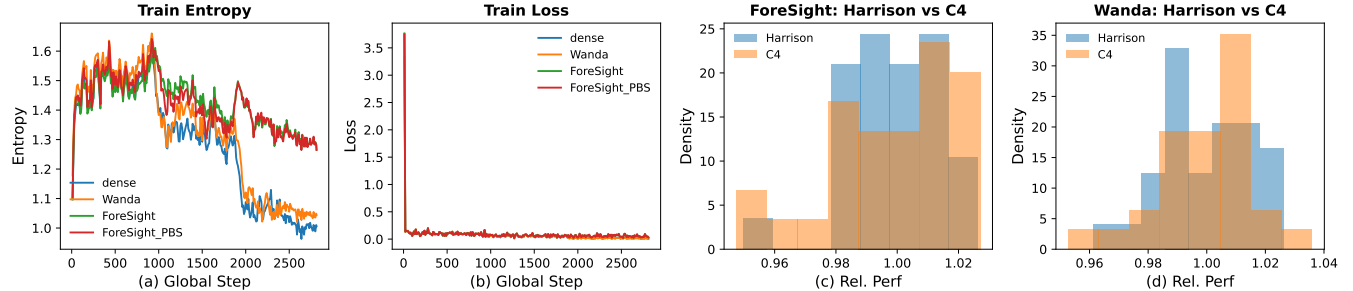


Figure 4: (a) Training entropy on Qwen3-8B (Health): dense LoRA (and LoRA+Wanda) exhibits a late-stage entropy collapse, while FORESIGHT and FORESIGHT+PBS maintain higher entropy throughout finetuning. (b) Training loss on Qwen3-8B (Health). (c–d) Domain-calibration ablation on Qwen3-0.6B at 30% sparsity: relative-performance distributions over 30 seeds on health tasks largely overlap when calibrating on Harrison (health) versus C4 (general) for (c) FORESIGHT and (d) Wanda.

Domain Calibration Does Not Improve Pruning While calibration data can materially affect pruning outcomes in general-purpose settings [Williams and Aletras, 2023; Bandari *et al.*, 2024; Ji *et al.*, 2024; Mitra *et al.*, 2024], Figures 4(c) and (d) show that, at 30% sparsity, using a health domain calibration set (Harrison) versus a general-domain set (C4) produces nearly identical distributions of relative performance on our health domain evaluation tasks for both ForeSight and Wanda. To control for confounders, we apply each pruning method to the same fully finetuned Qwen3-0.6B model and use matched calibration budgets across datasets (same number of sequences and context length). Across 30 random seeds, the histograms largely overlap with no consistent shift favoring Harrison, suggesting that domain-specific calibration provides no clear benefit in this setting.

Loss–Entropy Balance To explain the gains in health summarization and perplexity, we analyze Qwen3-8B training dynamics. In Fig. 4(b), FORESIGHT+PBS closely follows the dense-LoRA loss curve, indicating that pruning and recovery do not disrupt optimization. In Fig. 4(a), dense LoRA (and LoRA+Wanda) shows a late-stage entropy collapse, whereas FORESIGHT, especially FORESIGHT+PBS, maintains higher entropy throughout finetuning. This indicates a less over-confident output distribution, consistent with improved generation quality while preserving strong in-domain perplexity.

Domains Matter More Than Tasks. Given the performance gap we observe when transferring general purpose pruning across domains, we ask whether pruning strategies

should be organized by task type or by domain. We probe this question by comparing the geometry of LoRA adapters. For each layer, we compute Grassmann distances between the 8-dimensional leading eigenspaces (i.e., the learned low-rank adapter subspaces) for both cross-domain and within-domain model pairs, evaluated at the corresponding weight matrix. As shown in Fig. 3(d), task similar but cross domain pairs, Legal versus Health and CaseHold versus PubMedQA, concentrate at noticeably larger distances, while task diverse but intra domain pairs, Legal versus CaseHold and Health versus PubMedQA, cluster at smaller distances. This separation indicates that domain identity, rather than task type, more strongly determines the subspace directions emphasized by finetuning, reinforcing the need for domain aware pruning strategies.

6 Conclusion

We introduce **EfficientXpert**, a domain-aware pruning framework that transforms general-purpose LLMs into sparse, domain-specialized experts with minimal overhead. By integrating the propagation-aware *ForeSight Mask* and the lightweight *Partial Brain Surgeon* update into LoRA finetuning, EfficientXpert enables a unified, end-to-end pruning and adaptation process. Our experiments in the health and legal domains show that EfficientXpert consistently outperforms existing pruning baselines across all sparsity levels, achieving performance comparable to the dense baseline at 40% and 50% sparsity. Moreover, EfficientXpert incurs only modest additional finetuning time relative to dense LoRA while maintaining essentially the same peak memory footprint.

References

[Anil *et al.*, 2023] Rohan Anil, Andrew M Dai, Orhan Firat, Melvin Johnson, Dmitry Lepikhin, Alexandre Passos, Siamak Shakeri, Emanuel Taropa, Paige Bailey, Zhifeng Chen, et al. Palm 2 technical report. *arXiv preprint arXiv:2305.10403*, 2023.

[Bai *et al.*, 2023] Jinze Bai, Shuai Bai, Yunfei Chu, Zeyu Cui, Kai Dang, Xiaodong Deng, Yang Fan, Wenbin Ge, Yu Han, Fei Huang, et al. Qwen technical report. *arXiv preprint arXiv:2309.16609*, 2023.

[Bandari *et al.*, 2024] Abhinav Bandari, Lu Yin, Cheng-Yu Hsieh, Ajay Kumar Jaiswal, Tianlong Chen, Li Shen, Ranjay Krishna, and Shiwei Liu. Is c4 dataset optimal for pruning? an investigation of calibration data for llm pruning. *arXiv preprint arXiv:2410.07461*, 2024.

[Dubois *et al.*, 2023] Yann Dubois, Chen Xuechen Li, Rohan Taori, Tianyi Zhang, Ishaaan Gulrajani, Jimmy Ba, Carlos Guestrin, Percy S Liang, and Tatsunori B Hashimoto. Alpacafarm: A simulation framework for methods that learn from human feedback. *Advances in Neural Information Processing Systems*, 36:30039–30069, 2023.

[Frantar and Alistarh, 2023] Elias Frantar and Dan Alistarh. Sparsegt: Massive language models can be accurately pruned in one-shot. In *International conference on machine learning*, pages 10323–10337. PMLR, 2023.

[Guo *et al.*, 2025] Haojie Guo, Junyu Gao, and Yuan Yuan. Enhancing low-rank adaptation with recoverability-based reinforcement pruning for object counting. In *Proceedings of the AAAI Conference on Artificial Intelligence*, volume 39, pages 3238–3246, 2025.

[Han *et al.*, 2015] Song Han, Huizi Mao, and William J Dally. Deep compression: Compressing deep neural networks with pruning, trained quantization and huffman coding. *arXiv preprint arXiv:1510.00149*, 2015.

[Hu *et al.*, 2022] Edward J Hu, Yelong Shen, Phillip Wallis, Zeyuan Allen-Zhu, Yuanzhi Li, Shean Wang, Lu Wang, Weizhu Chen, et al. Lora: Low-rank adaptation of large language models. *ICLR*, 1(2):3, 2022.

[Ji *et al.*, 2024] Yixin Ji, Yang Xiang, Juntao Li, Qingrong Xia, Ping Li, Xinyu Duan, Zhefeng Wang, and Min Zhang. Beware of calibration data for pruning large language models. *arXiv preprint arXiv:2410.17711*, 2024.

[Jin *et al.*, 2019] Qiao Jin, Bhuwan Dhingra, Zhengping Liu, William W Cohen, and Xinghua Lu. Pubmedqa: A dataset for biomedical research question answering. *arXiv preprint arXiv:1909.06146*, 2019.

[Li and Liang, 2021] Xiang Lisa Li and Percy Liang. Prefix-tuning: Optimizing continuous prompts for generation. *arXiv preprint arXiv:2101.00190*, 2021.

[Lu *et al.*, 2024] Lei Lu, Zhepeng Wang, Runxue Bao, Mengbing Wang, Fangyi Li, Yawen Wu, Weiwen Jiang, Jie Xu, Yanzhi Wang, and Shangqian Gao. All-in-one tuning and structural pruning for domain-specific llms. *arXiv preprint arXiv:2412.14426*, 2024.

[Mitra *et al.*, 2024] Pallavi Mitra, Gesina Schwalbe, and Nadja Klein. Investigating calibration and corruption robustness of post-hoc pruned perception cnns: An image classification benchmark study. In *Proceedings of the IEEE/CVF Conference on Computer Vision and Pattern Recognition*, pages 3542–3552, 2024.

[Park *et al.*, 2020] Sejun Park, Jaeho Lee, Sangwoo Mo, and Jinwoo Shin. Lookahead: A far-sighted alternative of magnitude-based pruning. *arXiv preprint arXiv:2002.04809*, 2020.

[Qin *et al.*, 2018] Zhuwei Qin, Fuxun Yu, Chenchen Liu, and Xiang Chen. How convolutional neural network see the world-a survey of convolutional neural network visualization methods. *arXiv preprint arXiv:1804.11191*, 2018.

[Song *et al.*, 2025] Zirui Song, Bin Yan, Yuhan Liu, Miao Fang, Mingzhe Li, Rui Yan, and Xiuying Chen. Injecting domain-specific knowledge into large language models: a comprehensive survey. *arXiv preprint arXiv:2502.10708*, 2025.

[Sun *et al.*, 2023] Mingjie Sun, Zhuang Liu, Anna Bair, and J Zico Kolter. A simple and effective pruning approach for large language models. *arXiv preprint arXiv:2306.11695*, 2023.

[Touvron *et al.*, 2023] Hugo Touvron, Louis Martin, Kevin Stone, Peter Albert, Amjad Almahairi, Yasmine Babaei, Nikolay Bashlykov, Soumya Batra, Prajjwal Bhargava, Shruti Bhosale, et al. Llama 2: Open foundation and fine-tuned chat models. *arXiv preprint arXiv:2307.09288*, 2023.

[Williams and Aletras, 2023] Miles Williams and Nikolaos Aletras. On the impact of calibration data in post-training quantization and pruning. *arXiv preprint arXiv:2311.09755*, 2023.

[Wu *et al.*, 2025a] Dongyue Wu, Zilin Guo, Li Yu, Nong Sang, and Changxin Gao. Structural pruning via spatial-aware information redundancy for semantic segmentation. In *Proceedings of the AAAI Conference on Artificial Intelligence*, volume 39, pages 8368–8376, 2025.

[Wu *et al.*, 2025b] Zimeng Wu, Jiaxin Chen, and Yunhong Wang. Unified knowledge maintenance pruning and progressive recovery with weight recalling for large vision-language models. In *Proceedings of the AAAI Conference on Artificial Intelligence*, volume 39, pages 8550–8558, 2025.

[Yang *et al.*, 2023] Hongyang Yang, Xiao-Yang Liu, and Christina Dan Wang. Fingpt: Open-source financial large language models. arxiv. *arXiv preprint arXiv:2306.06031*, 2023.

[Zhang *et al.*, 2023] Mingyang Zhang, Hao Chen, Chunhua Shen, Zhen Yang, Linlin Ou, Xinyi Yu, and Bohan Zhuang. Loraprune: Pruning meets low-rank parameter-efficient fine-tuning. *ICLR*, 2023.

[Zhang *et al.*, 2024] Nan Zhang, Yanchi Liu, Xujiang Zhao, Wei Cheng, Runxue Bao, Rui Zhang, Prasenjit Mitra, and Haifeng Chen. Pruning as a domain-specific llm extractor. *arXiv preprint arXiv:2405.06275*, 2024.

[Zheng *et al.*, 2021] Lucia Zheng, Neel Guha, Brandon R Anderson, Peter Henderson, and Daniel E Ho. When does pretraining help? assessing self-supervised learning for law and the casehold dataset of 53,000+ legal holdings. pages 159–168, 2021.

[Zhou *et al.*, 2024] Zhi Zhou, Jiang-Xin Shi, Peng-Xiao Song, Xiao-Wen Yang, Yi-Xuan Jin, Lan-Zhe Guo, and Yu-Feng Li. Lawgpt: A chinese legal knowledge-enhanced large language model. *arXiv preprint arXiv:2406.04614*, 2024.

A A. An illustration of error propagation

Illustrative Example. Consider the following matrix multiplication sequence involving two consecutive linear layers:

$$\underbrace{\begin{bmatrix} 3 & 6 \end{bmatrix}}_X \cdot \underbrace{\begin{bmatrix} 2 & 2 \\ 4 & 1 \end{bmatrix}}_{W_1} \cdot \underbrace{\begin{bmatrix} 4 & 4 \\ 8 & 1 \end{bmatrix}}_{W_2} = \begin{bmatrix} 192 & 115 \end{bmatrix}.$$

The *local loss* is defined as $\|X \cdot (M \odot W_1 - W_1)\|_F^2$, and the *downstream loss* as $\|X \cdot (M \odot W_1 - W_1) \cdot W_2\|_F^2$, where M is the binary mask. Now consider pruning two different weights in W_1 .

Pruning entry $W_{1,1} = 2$ (Mask 1) results in a local loss of 36 and a downstream loss of 1152. In contrast, pruning entry $W_{2,2} = 1$ (Mask 2) yields the same local loss of 36, but a significantly larger downstream loss of 2340. This toy example illustrates that pruning decisions which are indistinguishable under local error metrics may lead to dramatically different downstream errors due to *error propagation*. As layer depth increases, this effect compounds, motivating the need for pruning strategies that can *foresee* such interactions.

B B. ForeSight for Attention and MLP

ForeSight extends to self-attention by pruning the *query* (Q) and *key* (K) projections *jointly*. Throughout, let $X \in \mathbb{R}^{l \times d}$ denote the flattened input activations of a calibration batch ($l = b \times s$, where b is the batch size and s the per-sample sequence length).

Weights and adapters.

- Base projections: $W^Q, W^K \in \mathbb{R}^{d \times d_k}$ and $W^V \in \mathbb{R}^{d \times d_v}$.
- LoRA adapters: $B^Q, B^K \in \mathbb{R}^{d \times r}$, $A^Q, A^K \in \mathbb{R}^{r \times d_k}$ and B^V, A^V for the value path.

The effective projections are $\widetilde{W}^Q = W^Q + B^Q A^Q$ and $\widetilde{W}^K = W^K + B^K A^K$.

Two-layer interaction. The attention “kernel” observed by the softmax is

$$X \widetilde{W}^Q \widetilde{W}^{K\top} X^\top.$$

Masking the Q projection. With a binary mask $M^Q \in \{0, 1\}^{d \times d_k}$ and sparsity constraint $\|M^Q\|_0 \leq k$, ForeSight selects the k coordinates whose removal minimizes the forward error

$$\min_{M^Q} \|X [\widetilde{W}^Q - M^Q \odot \widetilde{W}^Q] \widetilde{W}^{K\top}\|_F^2.$$

A second-order approximation yields the importance score

$$\Delta \mathcal{L}_{ij} \propto |\widetilde{W}_{ij}^Q| \|\widetilde{W}_{j,:}^K\|_2 \|X_{:,i}\|_2.$$

Masking the K projection. An analogous problem is solved for $M^K \in \{0, 1\}^{d \times d_k}$:

$$\min_{M^K} \|\widetilde{W}^Q [\widetilde{W}^K - M^K \odot \widetilde{W}^K]^\top X^\top\|_F^2, \quad \|M^K\|_0 \leq k,$$

with score

$$\Delta \mathcal{L}_{ij} \propto |\widetilde{W}_{ij}^K| \|\widetilde{W}_{:,j}^Q\|_2 \|X_{:,i}\|_2.$$

These propagation-aware scores prune Q and K in one pass, ensuring that early-layer sparsity respects downstream attention dynamics.

Masking the output projection O . The attention output is projected back to the residual stream by $\widetilde{W}^O = W^O + B^O A^O \in \mathbb{R}^{d \times d}$. Its output is consumed by the MLP *input* of both the gate and up projections. We therefore weight each output coordinate by the average downstream sensitivity

$$\nu_u^O := \frac{1}{2} \left(\|\widetilde{W}_{:,u}^{\text{gate}}\|_2 + \|\widetilde{W}_{:,u}^{\text{up}}\|_2 \right), \quad u \in [d],$$

and score each entry of \widetilde{W}^O by

$$\Delta \mathcal{L}_{uv}^O \propto |\widetilde{W}_{uv}^O| \|X_{:,v}\|_2 \nu_u^O.$$

This matches the implementation $|\widetilde{W}^O| \odot X_{\text{hat}} \odot \nu^O$ (with broadcasting).

Masking MLP gate/up projections. For the gated MLP, let $\widetilde{W}^{\text{gate}}, \widetilde{W}^{\text{up}} \in \mathbb{R}^{d_{ff} \times d}$ and $\widetilde{W}^{\text{down}} \in \mathbb{R}^{d \times d_{ff}}$ denote the effective (projection + LoRA) weights. Both gate and up outputs are mapped back by $\widetilde{W}^{\text{down}}$, so we use the per-hidden-unit propagation norm

$$\nu_h^{\text{down}} := \|\widetilde{W}_{:,h}^{\text{down}}\|_2, \quad h \in [d_{ff}].$$

Ignoring elementwise nonlinearities (Appendix C), ForeSight assigns the importance scores

$$\Delta \mathcal{L}_{hi}^{\text{gate}} \propto |\widetilde{W}_{hi}^{\text{gate}}| \|X_{:,i}\|_2 \nu_h^{\text{down}},$$

$$\Delta \mathcal{L}_{hi}^{\text{up}} \propto |\widetilde{W}_{hi}^{\text{up}}| \|X_{:,i}\|_2 \nu_h^{\text{down}}.$$

C C. Derivation of ForeSight importance Score

Let $\mathbf{X} \in \mathbb{R}^{m \times d}$ be a fixed data matrix and let $\mathbf{U}_1 = \mathbf{W}_1 + \mathbf{B}_1 \mathbf{A}_1 \in \mathbb{R}^{d \times h}$, $\mathbf{U}_2 = \mathbf{W}_2 + \mathbf{B}_2 \mathbf{A}_2 \in \mathbb{R}^{h \times p}$ be the (affine, bias-free) effective weight matrices of two consecutive linear layers. Define the loss

$$\mathcal{L}(\mathbf{U}_1) = \|\mathbf{X} \mathbf{U}_1 \mathbf{U}_2\|_F^2 = \text{Tr}(\mathbf{U}_2^\top \mathbf{U}_1^\top \mathbf{X}^\top \mathbf{X} \mathbf{U}_1 \mathbf{U}_2).$$

Fix an entry $\theta = \mathbf{U}_1[i, j]$. We study the loss change $\Delta \mathcal{L}_{ij}$ obtained by setting this entry to zero while *keeping all other parameters constant*. Throughout we assume (i) \mathbf{X} and \mathbf{U}_2 are constant during the perturbation, (ii) \mathbf{U}_1 corresponds to a first-order stationary point of \mathcal{L} (i.e. $\nabla_{\mathbf{U}_1} \mathcal{L} = \mathbf{0}$), and (iii) higher-than-second-order terms in a Taylor expansion are negligible for the magnitude of the perturbation considered.

Write $E_{ij} = e_i e_j^\top$, so that θE_{ij} extracts the affected entry. A standard matrix-calculus identity gives

$$\frac{\partial \mathcal{L}}{\partial \mathbf{U}_1} = 2 \mathbf{X}^\top \mathbf{X} \mathbf{U}_1 (\mathbf{U}_2 \mathbf{U}_2^\top), \quad (5)$$

$$\implies \frac{\partial \mathcal{L}}{\partial \theta} = 2 e_i^\top \mathbf{X}^\top \mathbf{X} \mathbf{U}_1 (\mathbf{U}_2 \mathbf{U}_2^\top) e_j. \quad (6)$$

Because \mathbf{U}_1 depends linearly on θ only through the i -th row, differentiation once more yields the diagonal Hessian entry

$$\frac{\partial^2 \mathcal{L}}{\partial \theta^2} = 2 e_i^\top \mathbf{X}^\top \mathbf{X} E_{ij} \mathbf{U}_2 \mathbf{U}_2^\top e_j = 2 (\mathbf{X}^\top \mathbf{X})_{ii} (\mathbf{U}_2 \mathbf{U}_2^\top)_{jj}.$$

Letting $\delta \theta = -\theta$ denote the pruning perturbation, a second-order Taylor expansion gives

$$\begin{aligned} \Delta \mathcal{L}_{ij} &= \mathcal{L}(\mathbf{U}_1 + \delta \theta E_{ij}) - \mathcal{L}(\mathbf{U}_1) \\ &= \underbrace{\frac{\partial \mathcal{L}}{\partial \theta}}_{=0} \delta \theta + \frac{1}{2} \frac{\partial^2 \mathcal{L}}{\partial \theta^2} (\delta \theta)^2 + O(\|\delta \theta\|^3) \\ &\approx \frac{1}{2} \theta^2 (\mathbf{X}^\top \mathbf{X})_{ii} (\mathbf{U}_2 \mathbf{U}_2^\top)_{jj}. \end{aligned} \quad (7)$$

Hence, under the stated assumptions, the *exact* second-order approximation to the loss increase is non-negative and is given by

$$\boxed{\Delta \mathcal{L}_{ij} \approx \frac{1}{2} \theta_{ij}^2 (\mathbf{X}^\top \mathbf{X})_{ii} (\mathbf{U}_2 \mathbf{U}_2^\top)_{jj} \quad (i \in [d], j \in [h])}.$$

This value serves as a principled importance score for weight pruning: the larger the product of the data-covariance entry $(\mathbf{X}^\top \mathbf{X})_{ii}$, the downstream energy $(\mathbf{U}_2 \mathbf{U}_2^\top)_{jj}$, and the squared weight magnitude θ_{ij}^2 , the greater the predicted loss incurred by zeroing θ_{ij} .

Nonlinearities in ForeSight can be safely ignored. In a preLayerNorm model, calibration pre-activations a is approximately standard normal, and the exact GELU has a slope in [-0.129, 1.129]. Thus, GELU only reweights token contributions by bounded factors, so our group selection by magnitudes is stable except for near ties. Empirically, the top k overlap between pre-activation and post-activation scoring is at least 90%.

D D. Training Dataset Construction

The domain training corpora are listed in Tables 5 and 6. For each domain, we stratify the original training split by label, shuffle with a fixed seed (1234), and subsample to the desired size. In PubMedQA, we retain only the *yes* and *no* classes because the released training set contains no *maybe* examples. For all other datasets, labels with too few instances are upsampled by sampling with replacement until the target count is reached. All training data and evaluation scripts follow the Alpaca template [Dubois *et al.*, 2023], with the full prompt formats listed in Appendix ??.

Table 5: **Health domain** training datasets with label distributions, shuffle settings, random seed, and sequence length.

Dataset	Label	Instances	Shuffle	Seed	Seq. Len.
MedNLI	entailment	2333	TRUE	1234	2048
	contradiction	2333		1234	2048
	neutral	2334		1234	2048
PubMedQA	yes	3500	TRUE	1234	2048
	no	3500		1234	2048
	maybe	0		1234	2048
HQS	-	1000	TRUE	1234	2048

Two domain-specific datasets are used in our experiments: **PubMedQA** and **CaseHold**. For **PubMedQA**, we sample 7,000 *yes* and 7,000 *no* examples; the *maybe* label is excluded due to lack of availability in the training split. For **CaseHold**, we sample 3,000 instances from each class label {0, 1, 2, 3, 4}. All dataset splits are shuffled once using a fixed seed

Table 6: **Legal domain** training datasets with label distributions, shuffle settings, random seed, and sequence length.

Dataset	Label	Instances	Shuffle	Seed	Seq. Len.
ContractNLI	entailment	2100	TRUE	1234	2048
	contradiction	1200		1234	2048
	neutral	2700		1234	2048
CaseHold	0	1400	TRUE	1234	2048
	1	1400		1234	2048
	2	1400		1234	2048
	3	1400		1234	2048
	4	1400		1234	2048
BillSum	–	1000	TRUE	1234	2048

E. Hyperparameters Settings

We provide all the hyperparameter used for training in Table 1, Table 2, and the two task specific domain model used in Section ???. For all dense Health domain models, we use training dataset described in Table 5 and the evaluation datasets described in Table 11. For all dense Legal domain models, we use training dataset described in Table 6 and the evaluation datasets described in Table 12. The training hyperparameter are set the be the same for PubMedQA model and CaseHold model with training datasets described in previous section. To note that all training are conducted on 4 NVIDIA A100 GPUs with 80GB memory. We adjust the per-device batch size and gradient accumulation steps to maintain a global batch size of 32.

Table 7: Dense Health Domain Training Hyperparameters

Hyperparameter	Value
model_name	meta-llama/Llama-2-7b-hf
learning_rate	1×10^{-4}
per_device_batch_size	2
gradient_accumulation_steps	4
num_train_epochs	3
weight_decay	0.01
fp16	True
save_steps	1000
max_seq_length	2048
lora_r	8
lora_alpha	16
lora_dropout	0
lora_bias	none
lora_target_modules	q.proj, o.proj, v.proj, k.proj, gate.proj, up.proj, down.proj
optimizer	torch.Adam

The LoRA training hyperparameter and training dataset used for EfficientXpert are identical to those used for the dense model to ensure a fair comparison. For ForeSight Mask, the mask learning rate is set to 0.5. For Partial Brain Surgeon, the regularization coefficient is set to 1×10^{-8} .

F. Evaluation Details

The name of the evaluation and number of instances in the test set are listed in Table 11 and Table 12. For all the eval-

Table 8: Dense Health Domain Training Hyperparameters

Hyperparameter	Value
model.name	meta-llama/Llama-2-7b-hf
learning_rate	1×10^{-4}
per_device_batch_size	2
gradient_accumulation_steps	4
num_train_epochs	3
weight_decay	0.01
fp16	True
save_steps	1000
max_seq_length	2048
lora_r	8
lora_alpha	16
lora_dropout	0
lora_bias	none
lora_target_modules	q.proj, o.proj, v.proj, k.proj, gate.proj, up.proj, down.proj
optimizer	torch.Adam

Table 9: Dense Legal Domain Training Hyperparameters

Hyperparameter	Value
model.name	meta-llama/Llama-2-7b-hf
learning_rate	1×10^{-4}
per_device_batch_size	2
gradient_accumulation_steps	4
num_train_epochs	3
weight_decay	0.01
fp16	True
save_steps	1000
max_seq_length	2048
lora_r	8
lora_alpha	16
lora_dropout	0
lora_bias	none
lora_target_modules	q.proj, o.proj, v.proj, k.proj, gate.proj, up.proj, down.proj
optimizer	torch.Adam

ations, we adopt the Alpaca template [Dubois *et al.*, 2023] to evaluate the performance of the models. All Alpaca templates are listed in Appendix ??.

G. Further Analysis

The Grassmann distance between two LoRA adapters of the same weight, parameterized by (B_1, A_1) and (B_2, A_2) respectively, is given by

$$d(U_1, U_2) = \left(\sum_{i=1}^r \cos^{-1}(\sigma_i)^2 \right)^{\frac{1}{2}}, \quad (8)$$

$$\text{where } B_1 A_1 = U_1 \Sigma_1 V_1^\top, \quad B_2 A_2 = U_2 \Sigma_2 V_2^\top. \quad (9)$$

and σ_i are the singular values of $U_1^\top U_2$, $r = 8$ for our experiment.

To understand how is task information encoded in the LoRA adapter, we further analyze the projection energy of each domain-specific or task-diverse model introduced in Section ??, as shown in Figure 5. For each model, we compute the projection energy of the LoRA adapters and average

Table 10: Dense Legal Domain Training Hyperparameters

Hyperparameter	Value
model_name	meta-llama/Llama-3-8b
learning_rate	1×10^{-4}
per_device_batch_size	1
gradient_accumulation_steps	8
num_train_epochs	3
weight_decay	0.01
fp16	True
save_steps	1000
max_seq_length	2048
lora_r	8
lora_alpha	16
lora_dropout	0
lora_bias	none
lora_target_modules	q_proj, o_proj, v_proj, k_proj, gate_proj, up_proj, down_proj
optimizer	torch.Adam

Table 11: Overview of health datasets used for evaluation.

	InternalMed_Harrison	MedNLI	PubMedQA	HQS
Domain	Health	Health	Health	Health
Task / Type	Generation	NLI	QA	Summarization
# Instances in Test	300	1422	500	100
Metrics	Perplexity	Acc & Macro-F1	Acc & Macro-F1	ROUGE

it by weight type. The plotted results reveal that the distribution of average projection energy exhibits **more consistent local patterns within the same task** (e.g., CaseHold vs. Legal or PubMedQA vs. Health), even when the domains differ.

For instance, **PubMedQA** and **Health**, although from different domains, both exhibit strong activation in `gate_proj` and `up_proj`. In contrast, **CaseHold** and **Legal** emphasize `k_proj` and `up_proj`. This pattern suggests that **task similarity plays a dominant role in shaping local projection energy patterns**, whereas **domain-level information may guide the broader global distribution**. These findings imply that LoRA adapters capture a **global structure governed by domain**, while their **local energy distribution reflects task-specific characteristics**, especially across components like attention, gate, up projection in MLP.

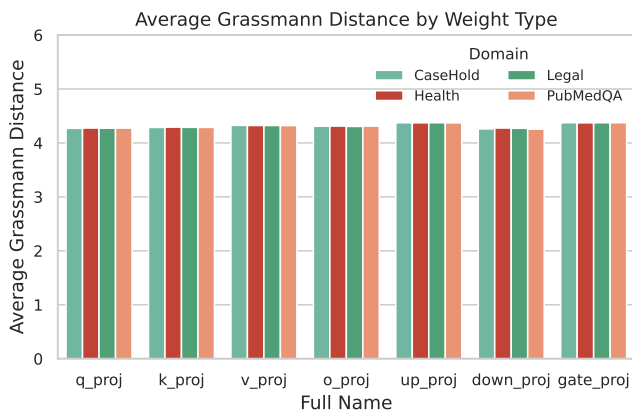


Figure 8: Grassmann distance between LoRA adapters and weight matrices by weight type.

Table 12: Overview of legal datasets used for evaluation.

	MultiLegalPile	ContractNLI	CaseHOLD	BillSum
Domain	Legal	Legal	Legal	Legal
Task / Type	Generation	NLI	QA	Summarization
# Instances in Test	300	1991	200	200
Metrics	Perplexity	Acc & Macro-F1	Acc & Macro-F1	ROUGE

These findings imply that while LoRA adapters may encode a global structure shaped by domain identity, task-specific characteristics drive significant variation in projection energy across weight types—particularly within attention and MLP components.

To further explore this contrast, we visualize the Grassmann distance between LoRA adapters and the corresponding base weight matrices for each layer. As shown in Figure 6, the Grassmann distances remain consistently high (above 4) across all layers and domains, indicating that LoRA adapters systematically amplify directions that diverge from the pre-trained model’s dominant subspaces. This pattern is mirrored in Figure 8, where all weight types exhibit similarly large distances.

These results suggest a fundamental duality: while the global subspace shift induced by LoRA is governed by domain-level signals—producing consistently large Grassmann distances—the local alignment revealed by projection energy varies according to task-specific usage patterns.

H Alpaca Templates

PubMedQA

Below is an instruction that describes a task related to healthcare, paired with detailed input from a scientific article.

Instruction: You are an expert clinician. Determine whether the following statement is correct.

Answer yes, no, or maybe.

Input: Contexts: {contexts}

Section Labels: {labels}

MeSH Terms: {meshes}

Question: {question}

Response: The answer is

MedNLI

Below is an instruction for analyzing clinical information.

Instruction: You are a licensed physician. Determine the logical relationship between two clinical statements based only on clinical knowledge and the given premise. Do not assume unstated facts.

Answer with exactly one label:

- entailment: the hypothesis must be true given the premise - contradiction: the hypothesis must be false given the premise - neutral:

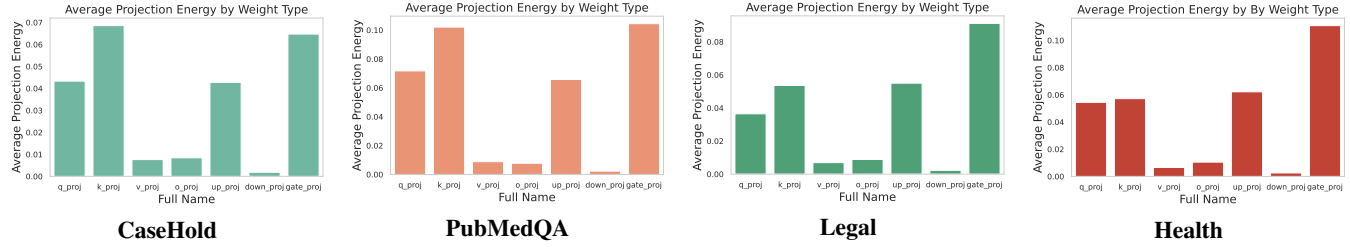


Figure 5: Projection energy by full name across domains.

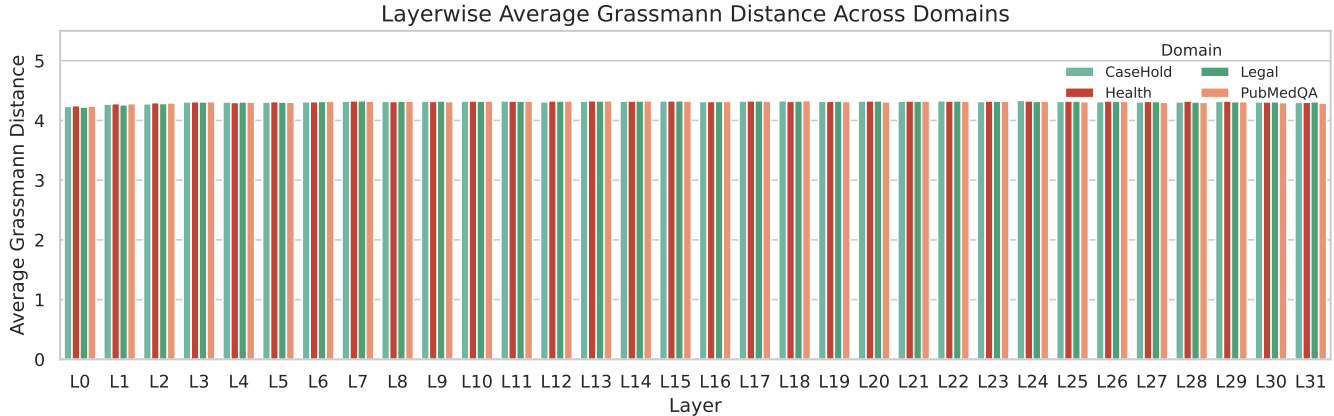


Figure 6: Grassmann distance between LoRA adapters and weight matrices across layers.

the hypothesis may be true or false given the premise

Input: Premise: {sentence1}

Hypothesis: {sentence2}

Response: The answer is

HQS

Below is an instruction that describes a task related to healthcare, paired with further context.

Instruction: Summarize the following consumer health question into a shorter version that preserves all critical information needed to answer it correctly. Keep key entities (e.g., conditions, treatments, tests) and the main intent. Remove peripheral details. Write a fluent sentence.

Input: {input_question}

Response: The shortened question is

CaseHold

Below is an instruction that describes a task related to legal reasoning.

Instruction: You are given a citing passage from a legal decision and five candidate holding statements. Select the holding statement that

best matches the citing passage. Focus on the specific legal rule, factual framing, and implication. Avoid choices that are merely topically similar.

Answer with a single integer in {0, 1, 2, 3, 4}.

Input: Citing passage: {citing_prompt}

0: {holding_0} 1: {holding_1}
2: {holding_2} 3: {holding_3} 4: {holding_4}

Response: The answer is

ContractNLI

Below is an instruction that describes a task related to contract analysis.

Instruction: Determine the relationship between the contract premise and the hypothesis. Answer with exactly one label: entailment, contradiction, or neutral. Consider all three options and base your decision only on the provided text.

Input: Premise: {sentence1}

Hypothesis: {sentence2}

Response: The answer is

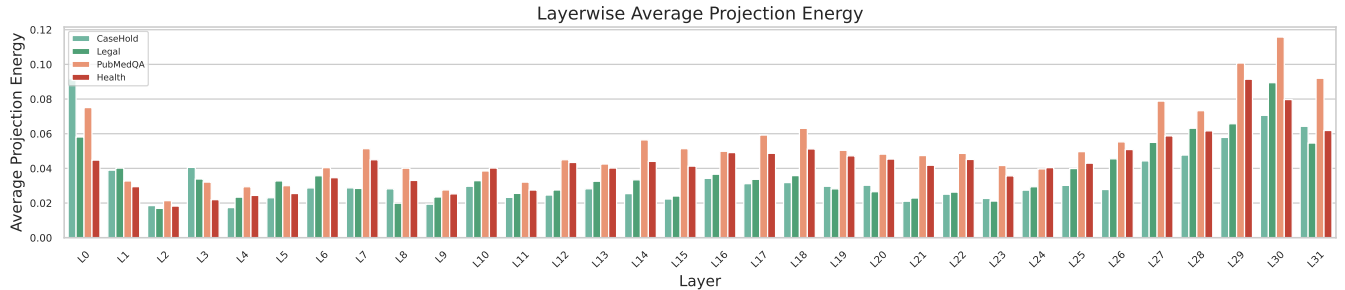


Figure 7: Projection energy across layers.

BillSum

Below is an instruction for summarizing a legislative bill.

Instruction: Summarize the following bill by explaining its major actions, purposes, and effects. Focus on what the bill aims to do and what changes it makes in practice. Paraphrase clearly for a general policy audience. Avoid quoting long spans or referencing subsection numbers unless needed.

Input: Bill Title: {title}

Bill Text: {input_text}

Response:

- **Llama-2-7b-hf:** The model is licensed under the LLaMA 2 community license.
- **Llama-3-8b:** The model is licensed under META LLaMA 3 community license.
- **PubMedQA:** The dataset is licensed under MIT license.
- **MedNLI:** The dataset is licensed under the Physionet Credentialed Health Data License Version 1.5.0.
- **HQS:** The dataset is licensed under Apache License 2.0.
- **CaseHold:** The dataset is licensed under Apache License 2.0.
- **ContractNLI:** The dataset is licensed under the CC BY 4.0 license.

H.1 Effect of Rank r on Partial Brain Surgeon

When the chosen rank r is substantially smaller than the number of pruned entries $|S_i|$, the resulting system becomes over-constrained, which can degrade downstream performance. To mitigate this, higher sparsity levels generally require a correspondingly larger rank r .

We evaluated the impact of varying r at 50% sparsity on Llama-3.2-1B. As shown in Figure 9, increasing the rank consistently improves relative performance. Each individual metric is recorded in table 13

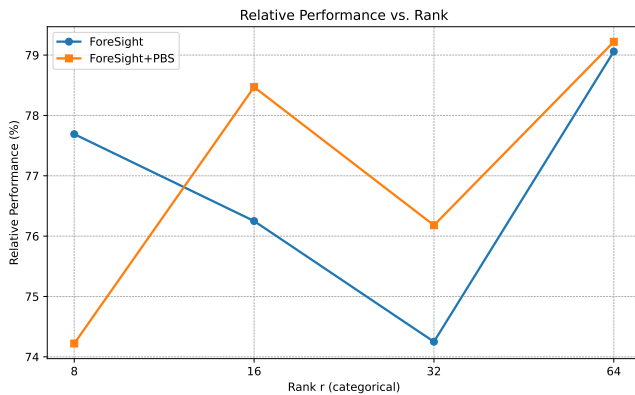


Figure 9: Relative performance of FourSight and FourSight + PBS at 50% sparsity on Llama-3.2-1B.

H.2 Discuss on the Artifacts

The license for the models and datasets used in this paper is as follows:

Table 13: Performance metrics for different methods at various ranks r at 50% sparsity on Llama-3.2-1B.

Method	Rank	Med PPL	MedNLI Acc	MedNLI F1	PubMedQA Acc	PubMedQA F1	HQS R1	HQS R2	HQS RL	Rel%
Dense	8	10.288	0.5605	0.5464	0.6800	0.4714	0.2476	0.0896	0.2204	—
	16	10.145	0.5956	0.5759	0.6600	0.4674	0.2609	0.0852	0.2343	—
	32	10.029	0.6069	0.5986	0.6660	0.4656	0.2507	0.0809	0.2284	—
	64	9.902	0.5872	0.5733	0.6500	0.4575	0.2439	0.0755	0.2122	—
ours	8	14.716	0.4286	0.3961	0.5200	0.3710	0.2171	0.0688	0.1948	77.69
	16	14.706	0.4286	0.3961	0.5200	0.3710	0.2171	0.0688	0.1948	76.26
	32	14.685	0.4197	0.3620	0.5205	0.3716	0.2114	0.0672	0.1914	74.26
	64	14.834	0.3926	0.3921	0.5300	0.3972	0.2201	0.0693	0.1974	79.06
oursPBS	8	15.854	0.3643	0.3412	0.5720	0.4027	0.1960	0.0568	0.1757	74.22
	16	15.020	0.4365	0.4252	0.5395	0.3845	0.2206	0.0637	0.1980	78.47
	32	14.908	0.3968	0.3979	0.5505	0.3917	0.2117	0.0641	0.1894	76.18
	64	15.106	0.3954	0.3824	0.5490	0.3910	0.2227	0.0688	0.1998	79.22